www.czasopisma.pan.pl PAN POLSKA AKADEMIA NAUK www.journals.pan.pl

Arch. Metall. Mater. **67** (2022), 2, 779-785

DOI: https://doi.org/10.24425/amm.2022.137818

HAITAO LIU[1,2,3], YUNHONG HUANG[4], WEI WANG[1,2,3*], ZIYANG ZHANG[1,2,3], HENGYAO DANG[5]

EFFECT OF SODIUM PENETRATION ON MICROSCOPIC DEFORMATION OF CARBON-BASED CATHODE MATERIALS DURING ALUMINUM ELECTROLYSIS

In this paper, the macroscopic and microscopic deformation caused by sodium penetration in the carbon cathode has been studied during aluminum electrolysis. The distributions of sodium concentration in the carbon cathode has been measured by SEM-EDS. The microstructure change caused by the gradient of the sodium concentration in the carbon cathode has been studied using transmission electron microscopy (TEM). The results indicate that sodium penetration decreases with the increase of the penetration depth. The stresses caused by the gradient of the sodium concentration result in a remarkable change for the microstructure of the carbon cathode. The formation of dislocations resulting in dislocation arrays and the development of kink band networks bring about material damage growth and possibly subsequent weakening of the cathode. These results can provide useful information that is helpful in developing an improved comprehending of the microscopic deformation mechanism of the carbon cathode during aluminum electrolysis.

Keywords: Carbon cathode; Microstructure; Sodium penetration; Dislocation; Kink band

1. Introduction

The industrial aluminum production is performed via the so called Hall-Heroult electrolysis process which began in 1886. Since then, this technology has been gradually improved in order to decrease energy consumption and environmental impacts. Due to sodium penetration into the carbon cathode materials, the early failure of carbon cathode blocks has a close relation with these two aspects [1,2]. The mechanism of sodium penetration into the carbon blocks is still not fully understood. The main transport mechanism is by interfacial diffusion, direct reduction and absorption [3,4]. For many years, several studies have focused on studying the influence of sodium expansion on the deformation of carbon cathodes during aluminum electrolysis. Zolochevsky was the first to measure the sodium expansion of semigraphitic cathode under three current density values and determine the relationship between the distribution of sodium concentration and time [5]. It has been previously reported that the sodium intercalation between graphite layers is responsible for the serious degradation of the cathode materials [6-8]. Indeed, sodium penetration has an adverse effect on the cell lining.

Recently, the deformation mechanism of graphite crystals has received much attention due to its effect on materials deterioration [9]. Hinks et al. systematically studied the effects of stresses on the microstructural development of the graphitic materials. They reported that displacing radiation resulted in the occurrence of kink bands and localized doming in graphite [10,11]. Based on molecular dynamics simulations, wang proposed that the graphite materials showed a law of three stages with extern load which include elastic deformation, microstructure rearrangement and microstructure compaction [12]. In these stages, microstructure rearrangement consists of bending, self-folding and flake-rotation. Because the bond strength between graphene sheets is relatively weak, graphite materials deform by basal plane slip and kink band formation, which can easily cause to pile up if indented. Gruber proposed a new micromechanism in the deformation of layer solids that ripplocation-mediated deformation could cause kinking non-linear elastic behavior [13].

According to theoretical calculations and experiments, the sodium penetration affected a remarkable change for the distribution of the first principal stress and the axial stress [5,14]. However, to the authors' best knowledge, a comprehensive

[1] HENAN UNIVERSITY OF SCIENCE AND TECHNOLOGY, COLLEGE OF MATERIALS SCIENCE AND ENGINEERING, LUOYANG 471023, CHINA
[2] COLLABORATIVE INNOVATION CENTER OF NONFERROUS METALS HENAN PROVINCE, LUOYANG 471023, CHINA
[3] HENAN KEY LABORATORY OF NON-FERROUS MATERIALS SCIENCE & PROCESSING TECHNOLOGY, LUOYANG 471023, CHINA
[4] HENAN UNIVERSITY OF SCIENCE AND TECHNOLOGY, ENGINEERING TRAINING CENTER, LUOYANG 471023, CHINA
[5] LUOYANG SHIP MATERIAL RESEARCH INSTITUTE, LUOYANG 471023, CHINA

* Corresponding author: wwlyzwkj@126.com

investigation of the microstructure changes of carbon blocks at nanoscales caused by sodium penetration is still lacking in some relevant knowledge. The purpose of this work is to investigate microstructural changes that are caused by sodium penetration induced mechanical deformation behaviour of the carbon cathode during aluminum electrolysis. In this work, by virtue of detailed scanning electron micrograph (SEM), energy dispersive spectrum analysis (EDS) and transmission electron microscopy (TEM), the distribution of sodium concentration, the contraction in the basal planes and kinking nonlinear elastic have been systematically investigated. This paper has direct application to comprehend sodium penetration damage for carbon cathodes.

2. Experimental

2.1. Materials and Chemicals

Cryolite, CaF_2, Al_2O_3 and NaF used in this experiment were derived from Sanxing Chemical Reagents Factory (Beijing, China) [15]. Before weighing, the raw materials were dried in a drying box at 150°C for 8 h. Standard experimental conditions are the total electrolyte mass of 200 g corresponding to the cryolite ratio (molecular ratio of NaF/AlF_3) of 4.0, 5% CaF_2 and 8% Al_2O_3.

The cathode samples were synthesized from 24% electrocalcined anthracites, 56% graphite and 20% coal tar pitch binder. The powders were pressed into molds of 25 mm diameter × 60 mm length under die-pressing at 20 MPa. The green samples were sintered at 1200°C in a vessel packed with fresh coke powders.

2.2. Experimental devices and methods

The laboratory-scale electrolytic cell and experimental procedure for aluminum electrolysis is similar to that in Reference 3. The cell is shown in Fig. 1. The strain of the carbon cathode caused by sodium penetration was determined by a LVDT(Linear Variable Differential Transformer) transducer (range 10 mm, resolution 1 μm). The cathode specimen was glued to the cathode lead by carbon glue. Cathode and electrolyte are set in a graphite crucible (anode) with a corundum cylinder side lining. The electrical current flowed through the anode lead, side of the anode, and melt to the cathode. To prevent the short circuit, a boron nitride plate was placed on the bottom of the graphite crucible.

The experiments were carried out in this furnace that was flushed with air gas and a small gas flow was maintained through the furnace to avoid air burn of the cell during electrolysis. The current is generated by a DC power supply and the cathode electric current density is 0.45 A/cm^2.

2.3. Characterization of specimens

The cathode samples were sectioned into two parts along their axis with a thin diamond saw after the end of the experiments. The elemental compositions of the surface of four regions of the half sample on the Na, F, Al, Ca contents were analyzed with scanning time of 90 seconds each 1 mm along its axis direction. And for inspection of their microstructure change, slices with dimensions 5 × 5 × 2 mm were cut around four points in Fig. 2 for preparing TEM samples. Then 3 mm disks

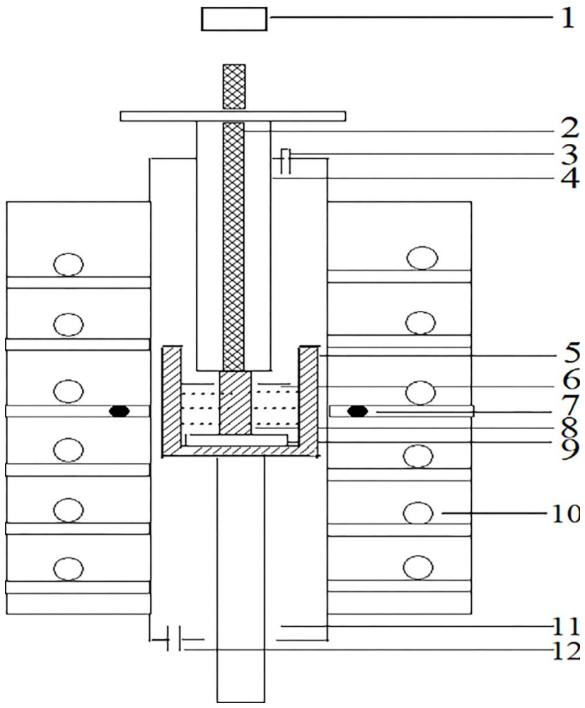

Fig. 1. The cell design for laboratory study. (1) LVD sensor. (2) Cathode current lead. (3) Gas outlet. (4) Cathode tube. (5) Anode (graphite crucible) (6) Electrolyte. (7) Thermocouples (8) Cathode. (9) Boron nitride plate. (10) Resistance wires. (11) Anode current lead. (12) Gas inlet

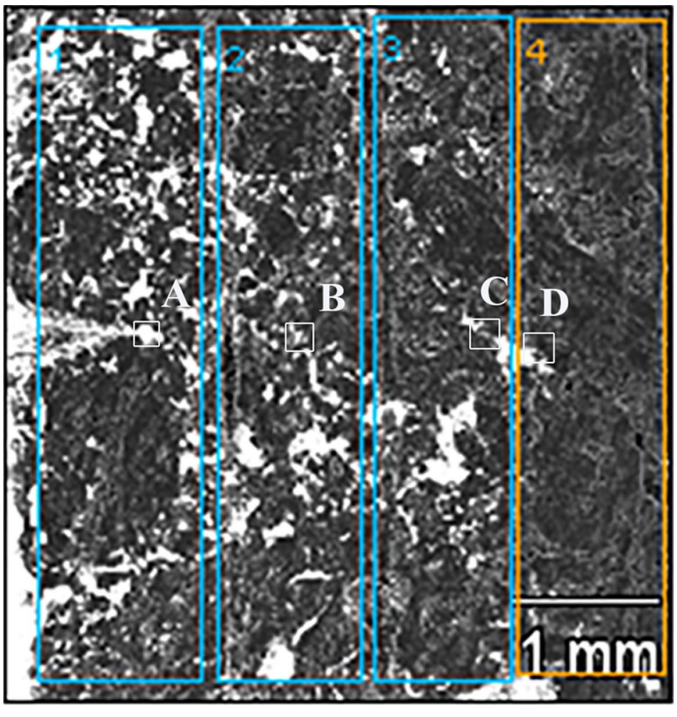

Fig. 2. Sketch map of SEM-EDS analysis of the carbon cathode

were prepared by mechanical polishing from above samples. To achieve the electron transparent region, the discs were thinned by ion milling on a Gatan precision ion polishing system 691. TEM observations were conducted using JEM-2100, operated at 200 kV.

3. Results and discussion

3.1. Sodium expansion measurement

During aluminum electrolysis sodium can create between aluminum and electrolyte according to the following reactions [16]:

$$Na_3AlF_6 \leftrightarrows 3NaF+AlF_3 \quad (1)$$

$$Al\ (l) + NaF\ (\text{in cryolite}) \leftrightarrows 3Na\ (\text{in C}) + AlF_3\ (\text{in cryolite}) \quad (2)$$

Fig. 3 indicates the curve of sodium expansion of the semigraphitic cathode during laboratory aluminum electrolysis against operating time. To obtain the exact results, 3 different samples have been taken to determine the sodium expansion with the same conditions. The standard deviation on the total sodium expansion is below 2%.

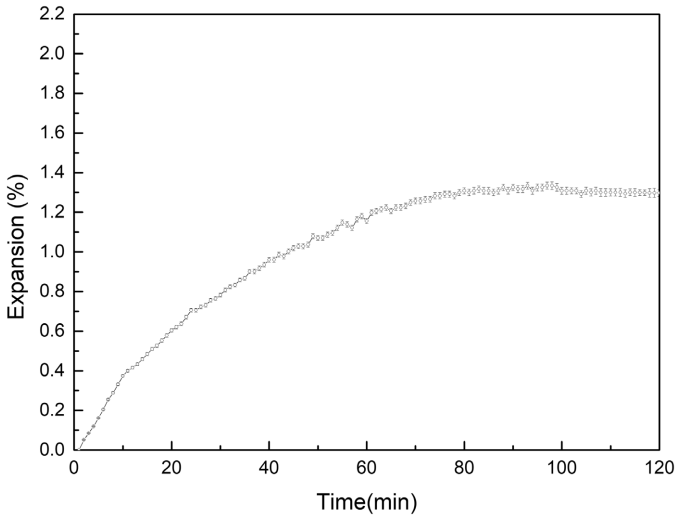

Fig. 3. Sodium expansion curve for the semigraphitic cathode sample during aluminum electrolysis with CR = 4.0 at 950°C

As indicated in Fig. 3, the sodium expansion rate is relatively high in the beginning of the electrolysis but slows down over time. This can be attributed to more and more Na penetration into the inner area of the graphite cathodes and increasing the sodium expansion in the cathodes. The sodium expansion rate decreases over time, reaches the minimum value, and remains a constant finally in the end. The main reason is that Na in the carbon cathode has reached saturation after a period of time. To understand the microstructure change, the morphologies of the carbon cathodes before and after aluminum electrolysis were characterized by SEM in Fig. 4(a) and Fig. 4(b) respectively.

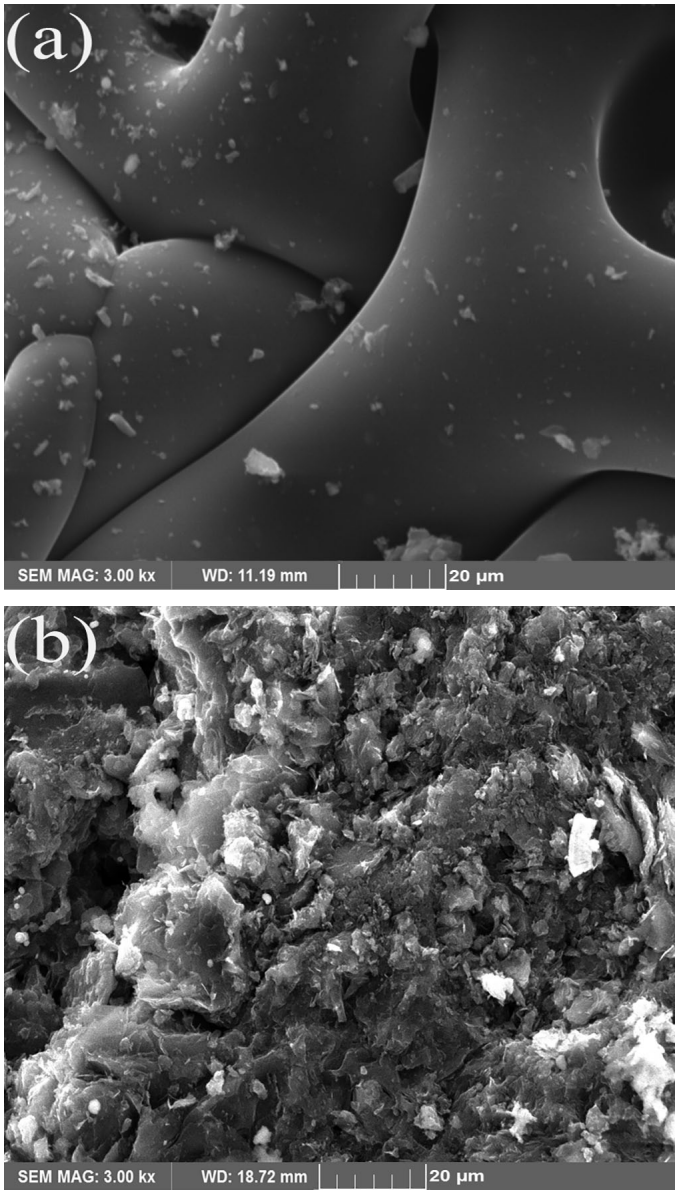

Fig. 4. Microstructures of the carbon cathodes (a) before electrolysis (b) after electrolysis

It can be seen that the pristine sample has a layered structure and smooth surface. Embellished with lots of white salts, the cathode sample exhibits a typical curled and corrugated morphology after electrolysis. Obviously, sodium and bath penetration lead to significant changes of the microstructure of the carbon cathode.

3.2. Penetration of sodium and melt in the cathode sample

EDS results of points A, B, C and D in Fig. 2 are shown in Fig. 5. It is known that the metallic Na and fluorides have penetrated into the cathode inner area. TABLE 1 lists the con-

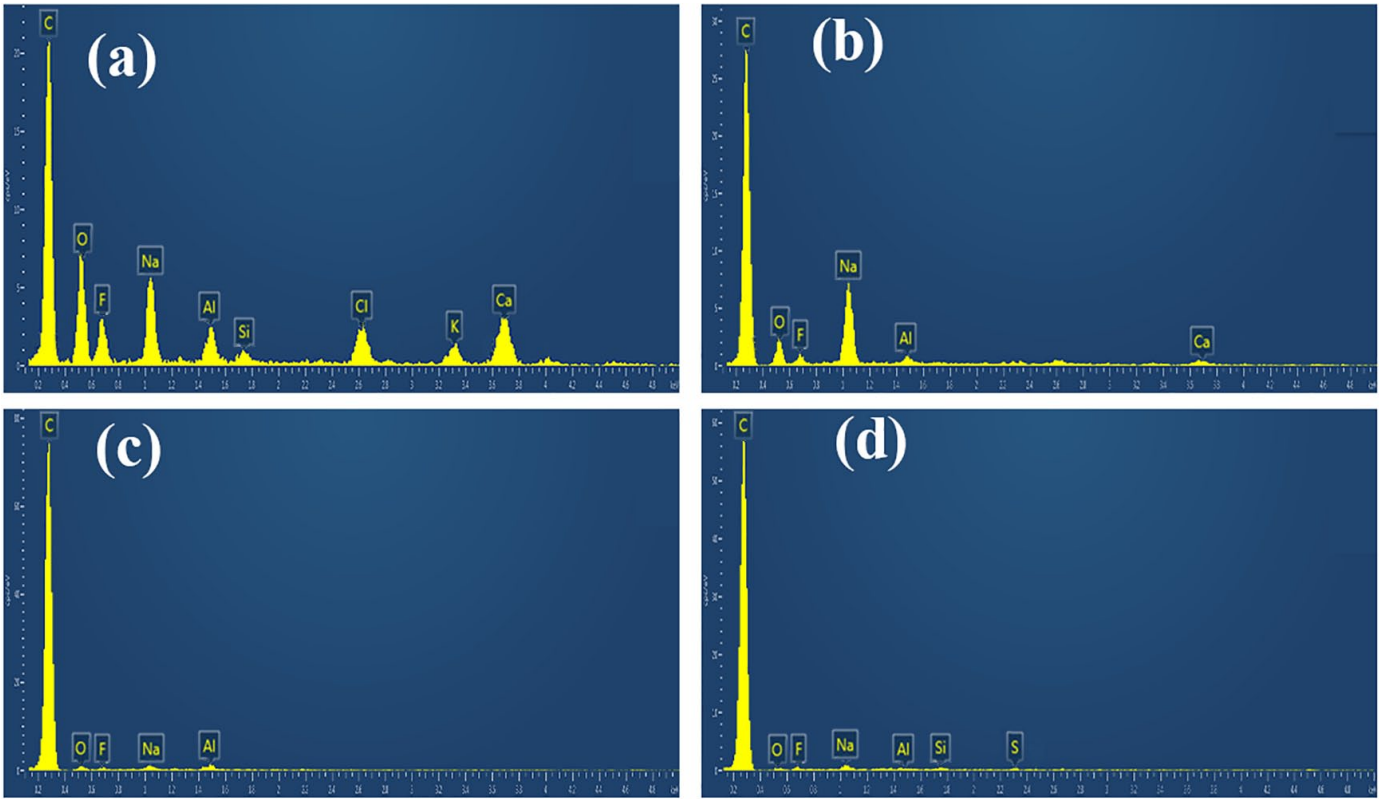

Fig. 5. EDS analysis of the carbon cathode

TABLE 1

The concentration of Na, F, Al and Ca in four different areas of the carbon cathode, wt%

Area	C	F	Na	Al	Ca	Other
1	80.01	13.16	3.61	1.72	1.22	0.28
2	90.02	4.66	2.74	1.39	0.82	0.37
3	94.22	2.37	1.84	0.85	0.38	0.34
4	96.45	1.38	1.16	0.58	0.21	0.22

centration of penetrated Na, F, Al and Ca in four different areas of the carbon cathode after electrolysis. It is obvious that the penetration amount of each element continuously decreased with increased penetration depth to the side of the cathode sample. Among them, the penetration amount of F is the largest, followed by Na; and both are larger than that of Al. There are two reasons for these. On the one hand, all fluoride (*i.e.*, NaF, CaF_2 and AlF_3) may penetrate into the region near the cathode surface. On the other hand, the generating Na through the reaction (2) may exist in the carbon cathode with elemental sodium and intercalation compounds ($C_{64}Na$) [17-20]. Although the mechanism of the sodium penetration into the carbon block is still not fully understood, it causes undoubtedly damage and fracture behavior of the carbon cathode. To further study the effect of sodium on the damage of the carbon cathode, the dislocation substructures of four different areas in the carbon cathode with various sodium concentrations were observed by TEM.

3.3. Effect of sodium concentrations on microstructural evolution of the carbon cathode

The TEM micrographs in Figs 6-9 show the structural changes observed in the carbon cathode after aluminum electrolysis. Also in these figures are sketch maps accounting for the microstructure of different areas in the carbon cathode with various sodium concentrations as it would occur if viewed parallel to the basal planes. These results provide a mechanism responsible for the microstructural deformation of the carbon cathodes during aluminum electrolysis. At a low sodium concentration of 1.16%, no remarkable structural changes can be observed except for zigzag contours in bottom – an example of such a outline is indicated in Fig. 6(a). This can be attributed to the vaporization of graphite edges that rebuild in the heat, in which the effect of Joule heat and the preferred current flow along specific edges play an important part. Moreover, the activation energy of atoms developing zigzag edges is lower than for other edge contours, which facilitates the formation of zigzag edges. In order to accommodate more atoms per unit area of basal plane in the regions with higher concentration of sodium, dislocations were to be created accordingly. With sodium concentration enrichment, dislocations parallel to the basal planes appear in the carbon cathode in Fig. 7(a), suggesting that they are moving on the basal planes. Because the dislocations will be of the same sign, they display a repelling force on each other with the joining of each additional dislocation making the existing dislocations to move so as to keep a balance segregation [21,22]. However, the dense forest dislocation structures are limited to the basal

planes, they do not entangle, and thus can move freely at a certain distances. Some time later, similarly spaced dislocations are formed to process across the grain developing a dislocation array as indicated in Fig. 7(b). At a sodium concentration of 2.74%, the dislocation array is suddenly transformed into a network of kink bands as indicated in Fig. 8(a).

Because of two independent slip systems only in graphite crystals, it is very difficult to generate plastic deformation in the carbon cathodes by slip. It is generally accepted that an increase in the dislocation density is beneficial to the development of kink band. Before the buckling graphene created a kink band, the dislocations had the highest energy [10]. When internal stresses caused by the gradient of the sodium concentration are high enough so that the dislocation separation changes less than a threshold value and kink bands form by buckling [23]. That is, deformation kink bands observed in carbon cathodes were due to a slow rotation of the lattice by the quick formation of pairs of dislocations on the basal plane. In addition, when the basal planes were loaded edge-on, they almost invariably failed by the development of kink bands. Below this critical defect separation, the dislocations tend to gravitate to others and it is very convenient for them to align vertically to develop a kink boundary as indicated in the change from Fig. 7(b) to Fig. 8(b) [24]. As the newly-formed boundaries are glissile, an increase in stress can result in a larger amount of 'kinking' in the grain structure to accommodate for the strain [25,26]. The symmetry of the kink band network showed that of a [0001] zone axis in graphite with the kink bands orientated at 60^{o} to each other as indicated in Fig. 9(b). The crystal axis of the largest kink bands ran parallel to the former dislocation array shown in Fig. 7(b) and thus also to the crystal boundary from which the dislocations were inserted. As indicated in Fig. 9(b) and Fig. 9(a), the width of the largest kink band increases evidently with the occurrence of dislocation networks. This can be attributed to the interaction

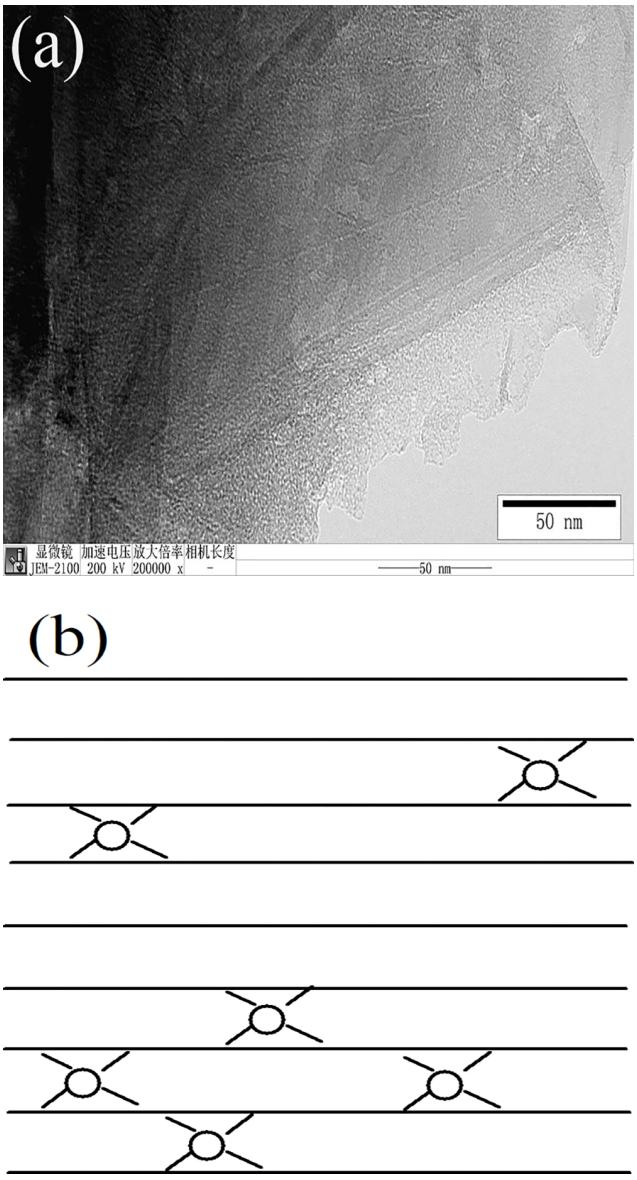

Fig. 6. (a) Sodium penetration induced structural modification in area 4 for the carbon cathode (b) explaining the evolution of the microstructure viewed parallel to the basal planes

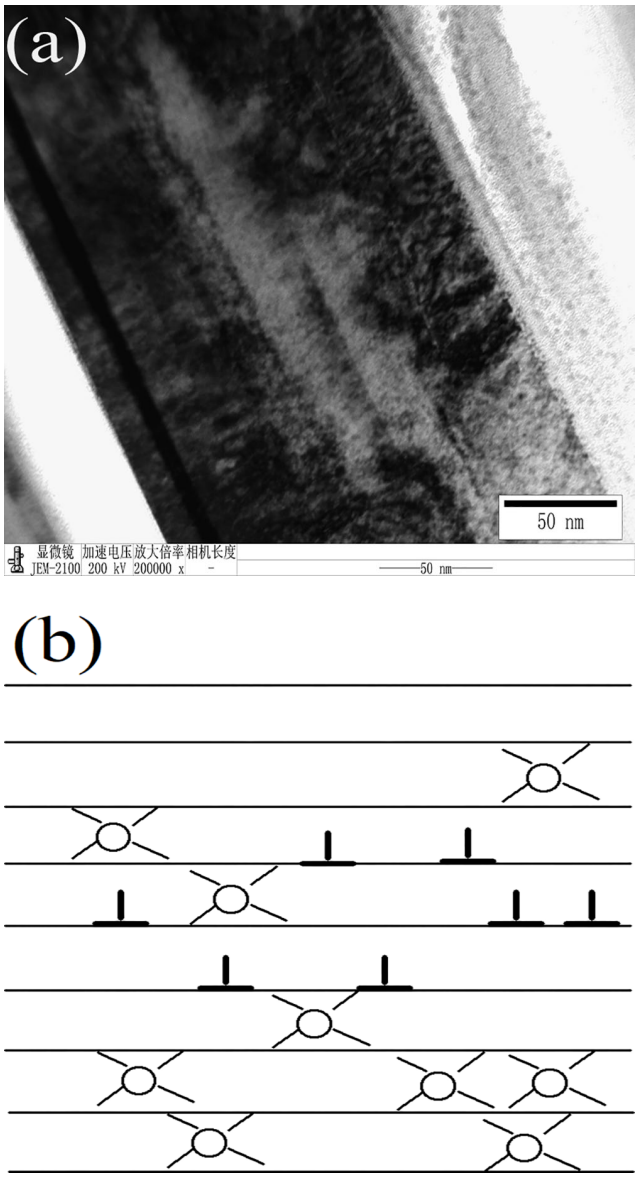

Fig. 7. (a) Sodium penetration induced dislocation array in area 3 for the carbon cathode (b) explaining the presence of the dislocation array

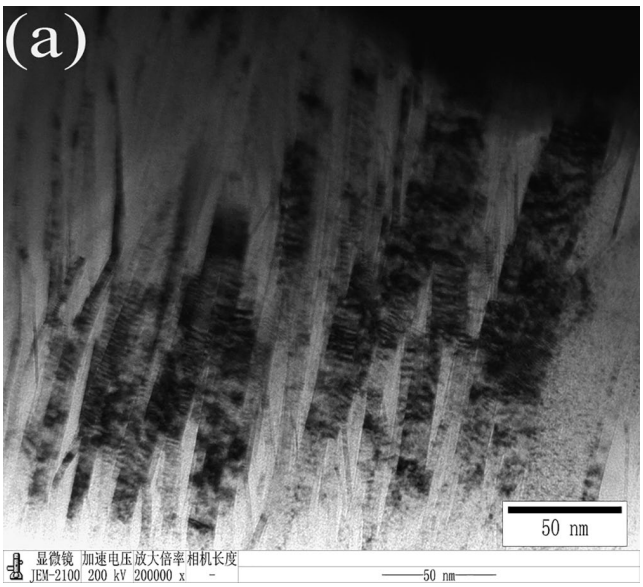

Fig. 8. (a) Sodium penetration induced kink bands in area 2 for the carbon cathode (b) explaining the presence of the kink bands

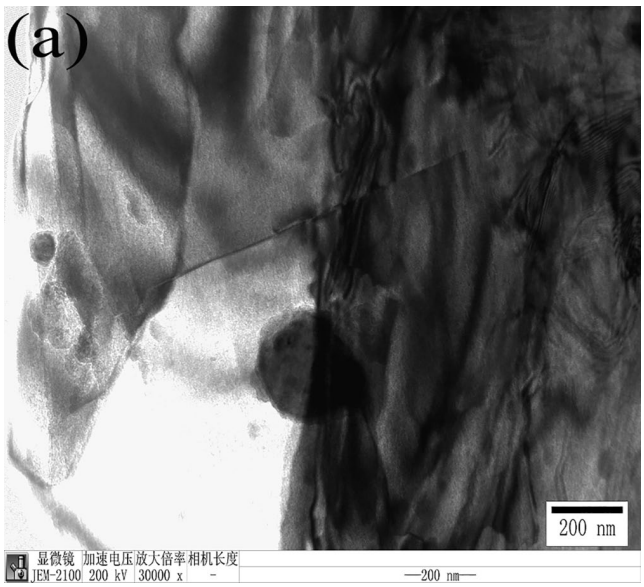

Fig. 9. (a) The 60°orientation relationship between kink bands induced by sodium penetration in area 1 for the carbon cathode (b) explaining the 60°orientation relationship between kink bands

between various dislocation arrays, basal plane slip bands, and dislocation region boundaries. Although the dislocation motion is often interrupted by interaction with the existing pinning sites, the residual strain acted as a driving force in the specimen makes it snag and free repeatedly [27-30]. In addition, most of flakes were subjected to sodium expansion damage in the form of fine fractured graphite, and the surface became rougher. With an increase in the stress caused by the gradient of the sodium concentration, a few of cracks occurred in the carbon cathode. In a word, the stress caused by the gradient of the sodium concentration has a significant effect on the microstructure of the carbon cathode.

4. Conclusion

Sodium penetration into the carbon cathode results in significant microstructure changes in the carbon cathode. The damage profile caused by the gradient of the sodium concentration in the carbon cathode has been studied during aluminum electrolysis. The following conclusions can be drawn from the current work.

The amount of Na penetration decreases with the increase of the depth of penetration into the carbon cathode.

The sodium expansion has a close relationship with the amount of Na penetration into the cathode. The sodium expansion enhances with the increase of the amount of Na penetration. When Na reaches saturation in the carbon cathode, the sodium expansion keeps a constant.

The imbalance distribution of stress caused by the gradient of the sodium concentration results in the dislocation production, motion and assembly into defect arrays and the appearance of the kink band network in the carbon cathode. This has an adverse impact on the carbon cathode.

Acknowledgements

The support from National Natural Science Foundation of China (NSFC) [grant number U1704154] was gratefully acknowledged.

REFERENCES

[1] L. Chauke, A.M. Garbers-Craig, Carbon **58**, 40-45 (2013).
[2] X. Lv, C. Guan, Z. Han, C. Chen, Journal of Molecular Liquids **298**, 112017 (2020).
[3] C. Ban, S. Zhu, X. Tao, W. Chen, Journal of Materials Science-Materials in Electronic **27**, 12074-12078 (2016).
[4] L.P. Lossius, H.A. Øye, Metallurgical & Materials Transactions B **31**, 1213-1224 (2000).
[5] A. Zolochevsky, J.G. Hop, G. Servant, T. Foosnæs, H.A. Øye, Carbon **41**, 497-505 (2003).
[6] P.Y. Brisson, H. Darmstadt, M. Fafard, A. Adnot, G. Servant, G. Soucy, Carbon **44**, 1438-1447 (2006).
[7] P.Y. Brisson, M. Fafard, G. Soucy, Canadian Metallurgical Quarterly **45**, 417-426 (2006).
[8] K. Tschope, C. Schoning, J. Rutlin, T. Grande, Metallurgical & Materials Transactions B **43**, 290-301 (2012).
[9] Picard, Fafard, Soucy, Bilodeau, JF, Materials Science & Engineering A **496**, 366-375 (2008).
[10] J.A. Hinks, G. Greaves, S.J. Haigh, C.-T. Pan, S.E. Donnelly, Materials Transactions **55**, 447-450 (2014).
[11] J.A. Hinks, S.J. Haigh, G. Greaves, F. Sweeney, C.T. Pan, R.J. Young, S.E. Donnelly, Carbon **68**, 273-284 (2014).
[12] W. Chao, C. Zhang, S. Chen, Carbon **109**, 666-672 (2016).
[13] J. Gruber, A.C. Lang, J. Griggs, M.L. Taheri, G.J. Tucker, M.W. Barsoum, Scientific Reports **6**, 33451 (2016).
[14] W. Wang, W. Chen, H. Liu, C. Zhang, Diamond and Related Materials **95**, 14-19 (2019).
[15] W. Wang, K. Sun, H. Liu, Construction and Building Materials **241**, 118119 (2020).
[16] E. Hjertenæs, A.Q. Nguyen, H. Koch, Physical Chemistry Chemical Physics **18**, 31431-31440 (2016).
[17] M. Anji Reddy, M. Helen, A. Groß, M. Fichtner, H. Euchner, ACS Energy Letters **3**, 2851-2857 (2018).
[18] W. Wang, K. Sun, Applied Sciences **10**, 2228 (2020).
[19] C. Kamal, A. Chakrabarti, A. Banerjee, S.K. Deb, Physica E:Low-Dimensional Systems and Nanostructures **54**, 273-280 (2013).
[20] C. Xia, S. Watcharinyanon, A.A. Zakharov, L.I. Johansson, R. Yakimova, C. Virojanadara, Surface Science **613**, 88-94 (2013).
[21] R. Krishna, A.N. Jones, L. Mcdermott, B.J. Marsden, Journal of Nuclear Materials **467**, 557-565 (2015).
[22] B. Lei, L. He, M. Yi, L. Ran, H. Xu, Y. Ge, K. Peng, Carbon **49**, 4554-4562 (2011).
[23] W. Wang, W. Chen, W. Gu, Materials Science & Engineering A **687**, 107-112 (2017).
[24] J.-F. Wen, S.-T. Tu, X.-L. Gao, J.N. Reddy, Materials Science & Technology **30**, 32-37 (2014).
[25] Y. Nakamura, K. Oohashi, T. Toyoshima, M. Satish-Kumar, J. Akai, Journal of Structural Geology **72**, 142-161 (2015).
[26] Q.Y. Lin, T.Q. Li, Z.J. Liu, Y. Song, L.L. He, Z.J. Hu, Q.G. Guo, H.Q. Ye, Carbon **50**, 2369-2371 (2012).
[27] V.A. Sethuraman, M.J. Chon, M. Shimshak, V. Srinivasan, P.R. Guduru, Journal of Power Sources **195**, 5062-5066 (2011).
[28] B. Wang, D.E. Wolfe, M. Terrones, M.A. Haque, S. Ganguly, A.K. Roy, Carbon **117**, 201-207 (2017).
[29] M. Liu, G. Wang, P. Xu, Y. Zhu, W. Li, Applied Sciences **10**, 3238 (2020).
[30] Y. Liu, H. Wang, K. Yang, Y. Yang, J. Ma, K. Pan, G. Wang, F. Ren, H. Pang, Applied Sciences **9**, 2677 (2019).